Supplementary Materials and Methods.

Chromatin immunoprecipitation

ChIP was performed as published (Ezhkova and Tansey, 2006), with modifications. Lysis buffer contain 150 mM NaCl. Cell lysis was by resuspending crosslinked cells in 400 µl lysis buffer containing 10 µl of 20 mg/ml Zymolyase T100 (Seikagaku Corp, Japan) and incubation at 37° until all cells were spheroplasted and lysed; 400 µl lysis buffer was added then tubes were spun at 20 000 g at 4° for 30 minutes and the supernatant discarded, with the pellet resuspended in 600 µl lysis buffer. Immunoprecipitation was with 10 µl anti-CTD antibody 8WG16 (Covance) for one hour resting on ice, then immunocomplexes were collected by incubation with washed protein G-agarose beads (Upstate) for 2 hours at 4° while rotating. DNA was quantitated by qPCR on an Applied Biosystems 7900 real time PCR machine, following manufacturer's protocols. Primers used: *ALD3*-F GCTTTAGGAACCCACATGGATA, *ALD3*-R TACCACCGCATTCTAGTGTGATA; *DHR2*-F CATCTGTTACCATATCCGGTGTT, *DHR2*-R GCTGATGTCTCCAAACTTTGACT; *HSP104*-F GCCACCACCAATAACGAATATAG, *HSP104*-R TGTTTGTCTCACACTTGGTTCAG; *HXT1*-F AGGCTGTCGGTTTAAGTGACTCT, *HXT1*-R CAACGGTGTACAGAGAACAACAA; *REX4*-F AATGGAGAACTTGGGTTAGTGGT, *REX4*-R GCCCTACAAGAATTCTACCTTCC; *SUC2*-F TGTTGGATCCTTCAATGGTACTC, *SUC2*-R GGGTCAGTGTTGAAGAAAGTTTG; *TUB2*-F CATGTCTGGTGTGACAACTTCAT, *TUB2*-R GTAGCCGACCATGAAGAAATGTA.

Ezhkova, E., and Tansey, W.P. (2006). Chromatin immunoprecipitation to study protein-DNA interactions in budding yeast. Methods Mol Biol *313*, 225-244.

Supplementary Figure Legends

Figure S1. Predominantly mononucleosomes from micrococcal nuclease digestions. Agarose gel of micrococcal nuclease digestions of chromatin from cultures before (0'), 20', or 60' post glucose addition.

Figure S2. (A) Dynamic Bayesian network representation of a hidden Markov model for predicting posterior probabilities of nucleosome formation. Squares indicate discrete nodes, circles indicate continuous nodes. Hidden nodes are shown with no background, while observed nodes are shaded. The model structure is shown for the first two 4 bp steps along the genome (the structure and parameters of the model are repeated as bp numbering increases from left to right). There are 37 nucleosome states in the H node, corresponding to the nucleosome length of 148 bp, and one linker state. H_{prior} is used to specify the initial probabilities for each state in the H node. In order to reduce the number of fitting parameters, all nucleosome states are mapped to one state of the "merge" (M) node, while the linker state is mapped to the other. The M node is connected to the G node which specifies the number of Gaussians used to model the empirical distribution of probe log intensities. Finally, the O node represents observed log intensities as a linear combination of Gaussians. **(B) The transition matrix of the hidden Markov model.** N_1 through N_{37} represent consecutive nucleosomal states (green circles), while L is the linker state (yellow circle). From the linker state a transition can be made to another linker state with probability P_{LL}, or to the first nucleosome state with probability $P_{LN} = 1 - P_{LL}$. Once a new nucleosome is started all subsequent nodes are placed with probability 1 until the next linker state is reached.

Figure S3. HMM accurately predicts published nucleosome positions. The HMM developed for this study was applied to a genome-wide data set of relative hybridization intensities of nucleosomal DNA obtained from glucose grown cells and the resulting HMM nucleosome predictions were compared to published positions over several regions (*CHA1*, *PHO5*, *STE6*, *BAR1*, *RE*, *MET16*, *MET17*). As all nucleosome starting probabilities tend to be clustered, all nucleosome starting probability values around a central peak were added together (P) and if this sum was greater than Pmin = 0.4 it was scored as 'nucleosome present'. X-axis represents distance between centres of HMM-predicted and published nucleosomes, and y-axis is the cumulative fraction of nucleosomes accounted for at a given center-to-center distance. "Uniform" represents average accuracy against published loci of multiple runs of randomly placed nucleosomes, constrained by steric hinderance, and error bars represent standard error.

Figure S4. Nucleosome positions do not change at the glucose-independent *CHA1* promoter. HMM nucleosome predictions at the indicated times prior (0 min) or post (20 and 60 minutes) glucose addition. Blue tracks represent predicted nucleosome occupancy, from unoccupied (0) to fully occupied (1). Green tracks represent the probability of initiating a nucleosome at that location. Previously determined in vivo nucleosome positions (Moreira and Holmberg, 1998) are shown as brown ovals at the bottom of the figure.

Figure S5. Multiple alternate nucleosome arrangements at the glucose-repressed *ARP2* gene. Nucleosome protection data, represented as the ratio of nucleosomal DNA to genomic DNA by tiling microarray (purple lines), HMM predictions of the probability of nucleosome

occupancy (blue lines) and HMM predictions of the probability of initiating a nucleosome (green lines) are shown for the *ARP2* promoter, diagrammed at the bottom, at the indicated times prior to (0 min) or post (20 and 60 minutes) glucose addition.

Figure S6. Nucleosome acquisition during repression at the *ADH2* promoter. Nucleosome protection data, represented as the ratio of nucleosomal DNA to genomic DNA by tiling microarray (purple lines), HMM predictions of the probability of nucleosome occupancy (blue lines) and HMM predictions of the probability of initiating a nucleosome (green lines) are shown for the *ARP2* promoter, diagrammed at the bottom, at the indicated times prior to (0 min) or post (20 and 60 minutes) glucose addition. Previously determined in vivo nucleosome positions for cells grown in glucose (Verdone *et al.,* 1996) are shown as brown ovals at the bottom of the figure.

Figure S7. Accurate glucose-induced nucleosome remodelling. For *ADH2* and *SUC2*, HMM-predicted nucleosome positions prior (0 min) or post (20 and 60 minutes) glucose addition compared to published nucleosome positions from cells grown in glucose (Gavin and Simpson, 1997; Verdone *et al*., 1996) as in Supplementary Figure 2.

Figure S8. A Nucleosome Depleted Region Resides at the 3' End of All Genes. *Top panel*: Nucleosome structure at transcription termination sites. Nucleosome occupancy for the 3' end of individual genes aligned relative to the transcriptional termination site (Nagalakshmi *et al.*, 2008) was clustered by K-means into four groups, and then sorted sequentially within each group by the position of the minimum occupancy value. *Bottom Panel*: Genome-wide average promoter

nucleosome profile. The nucleosome occupancies for the 3' ends of all genes were aligned relative to the transcription termination site, which is set as position 0, and then averaged at every nucleotide 500 bp upstream (internal to the gene) and 500 bp downstream over all genes to yield the average occupancy, which ranges from 0 (no nucleosome) to 1 (fully occupied).

Figure S9. Promoter nucleosome structures differ for weakly versus highly expressed genes. The 1000 most highly and weakly express genes, as determined by absolute intensity of mRNA hybridization to Agilent Microarrays (Zaman *et al.*, 2009), were filtered to eliminate dubious ORFs and transcripts not detected by Nagalakshmi *et al.*, 2008, resulting in 868 highly expressed genes (black line) and 210 weakly expressed genes (purple line). These were aligned by TSS and average nucleosome occupancy plotted for cells grown in glycerol prior to glucose addition, from no nucleosome (0) to fully occupied (1).

Figure S10. Nucleosome remodelling occurs infrequently during transcriptional reprogramming. Scatter plot showing the relationship between transcriptional change and nucleosome remodeling are presented as described in the legend to Figure 4, except that t-tests of changes in promoter nucleosomes in the graph designated "signal intensity" were based on promoter nucleosome density obtained directly from normalized hybridization values from microarrays and for those graphs labelled "occupancy" t-tests were based on HMM-predictions of nucleosome occupancy. Time points after glucose addition are as indicated.

Figure S11. Changes in RNA polymerase II levels correlated with changes in mRNA levels. (Left scale, broad bars) Fold change in RNA pol II levels within ORFs before and 20 minutes

after glucose addition as determined by ChIP, normalized to tubulin (*TUB2*). Black bars are promoters which undergo nucleosome remodeling events; gray bars are promoters with unchanged promoter nucleosome structure. Dashed horizontal lines are log scale. (Right scale, narrow hatched bars) Log2 change in mRNA levels before and 20 minutes after glucose addition, from Zaman *et al.* (2009).

Figure S12. Promoter nucleosome profiles exhibit limited alteration following glucose induction or repression. Average nucleosome occupancy (from no nucleosome, 0, to fully occupied, 1) was determined for the promoters of all genes induced (top) or repressed (bottom) 4-fold or more 20 minutes after glucose addition and plotted as a function of position from the transcription start site (TSS). Black lines: nucleosome occupancy prior to glucose addition; Purple lines: nucleosomes occupancy 20 min following glucose addition.

Figure S13. Changes in nucleosome occupancy at the 3' ends of genes are unrelated to transcriptional changes. (A) Changes in nucleosome occupancy at individual gene ends were aligned by TSS, clustered by K-means into three groups, and then sorted within each group. (B) Scatter plot showing the relationship between transcriptional change and nucleosome remodeling at the 3' end are presented. Each point represents a single gene with the x-axis providing a t-test of change in gene-end nucleosome density before and 20 minutes after glucose addition and the y-axis showing the log2 change in mRNA level before and 20 minutes after glucose addition. The r correlation between transcriptional change and the t-test nucleosome occupancy change is given.

Figure S14. Genes lacking TATA boxes have a more defined promoter nucleosome structure. The average nucleosome occupancy was calculated separately for the subset of genes containing a TATA-box (black line) and those lacking a TATA-box (purple line) and plotted as a function of the distance from the transcription start site.

Figure S15. Promoters with TATA boxes are more likely to undergo nucleosome remodelling. Scatter plot showing the relationship between transcriptional change and nucleosome remodeling are presented as described in the legend to Figure 4, except that t-tests of changes in promoter nucleosomes in the graph designed "signal intensity" were based on promoter nucleosome density obtained directly from normalized hybridization values from microarrays and for those graphs labelled "occupancy" t-tests were based on HMM-predictions of nucleosome occupancy. Genes are subdivided into those containing promoter TATA-boxes (red dots) and those whose promoters lack TATA-box (blue dots). Time points after glucose addition are as indicated.

Figure S16. Most occurrences of glucose-regulated motifs undergo little change in nucleosome occupancy. For all genes induced (upper panel) or repressed (lower panel) 4-fold or more 20 minutes after glucose addition, change in nucleosome occupancy directly over individual motifs were calculated from -1 (completely occupied at 0 min to completely unoccupied 20 min after glucose addition) to 1 (unoccupied at 0 min to occupied at 20 min). The density of individual data points is depicted in color-coded bins from 1 (all individual data points contained within bin) to 0 (no data points contained within bin). The average change and standard deviation for all occurrences of the motif within induced or repressed genes, as shown

in Figure 6, is provided for each motif. The bar labelled “intergenic” is the individual changes in nucleosome occupancy over all glucose-induced or repressed promoters.

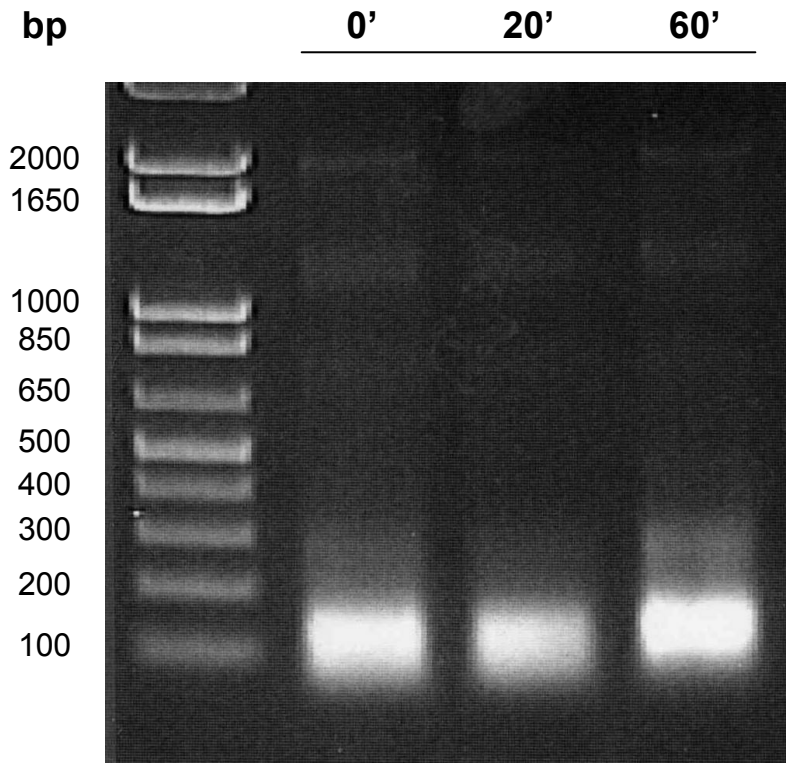

Zawadzki *et al*., Figure S1

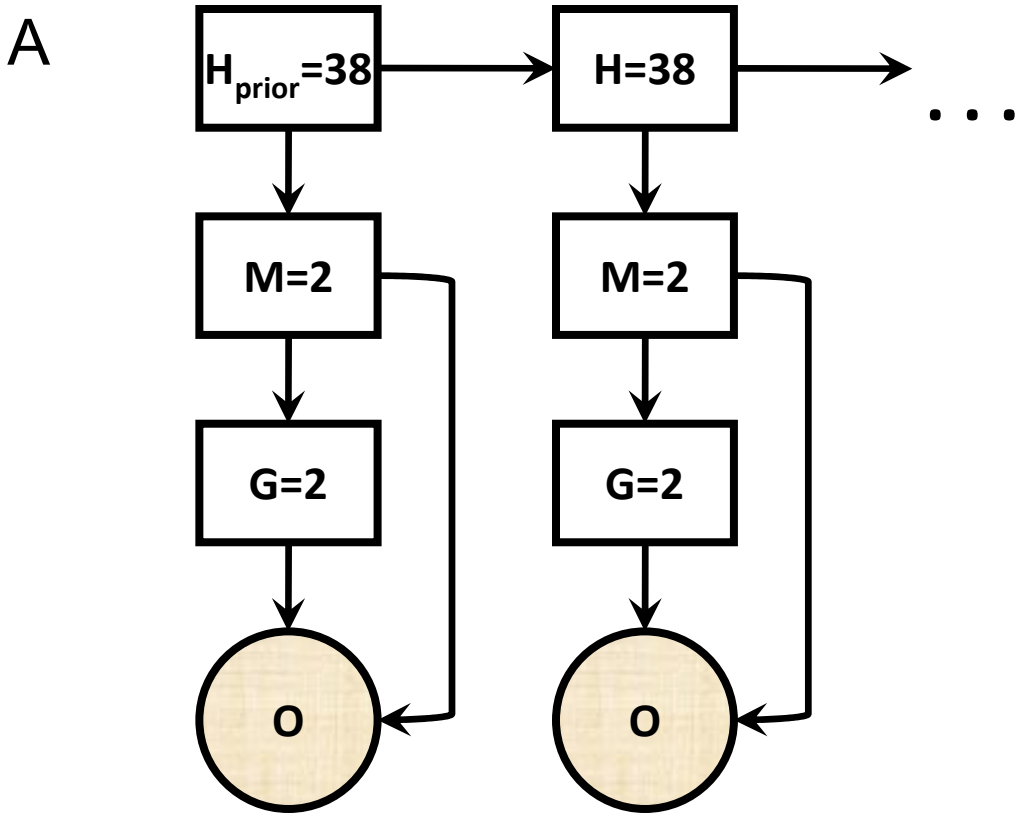

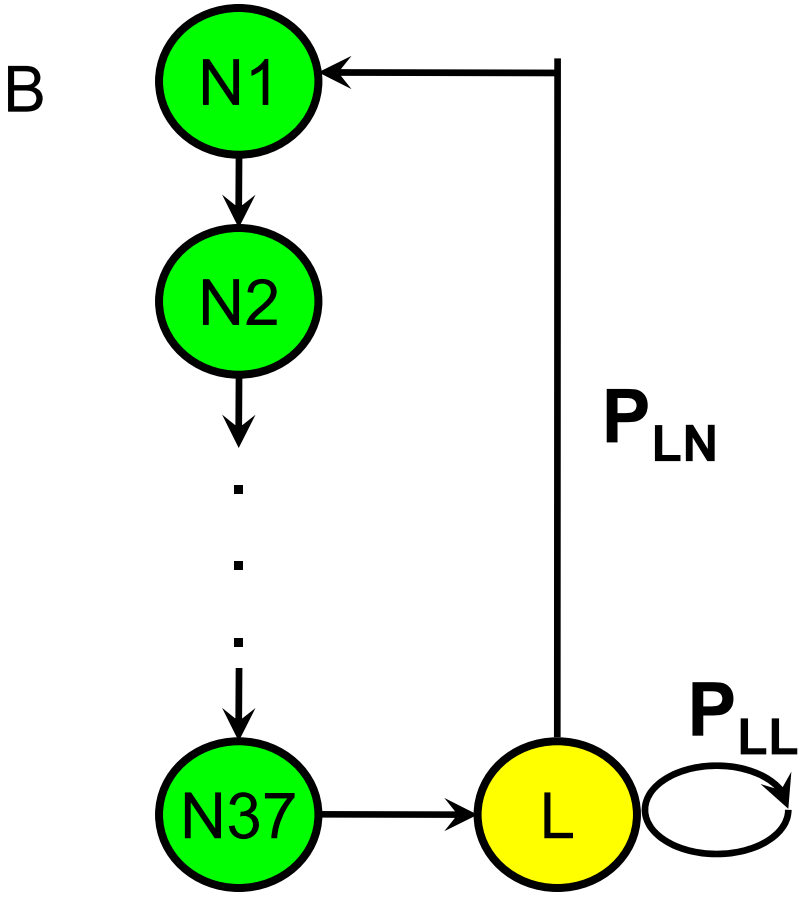

Zawadzki *et al.*,
Figure S2

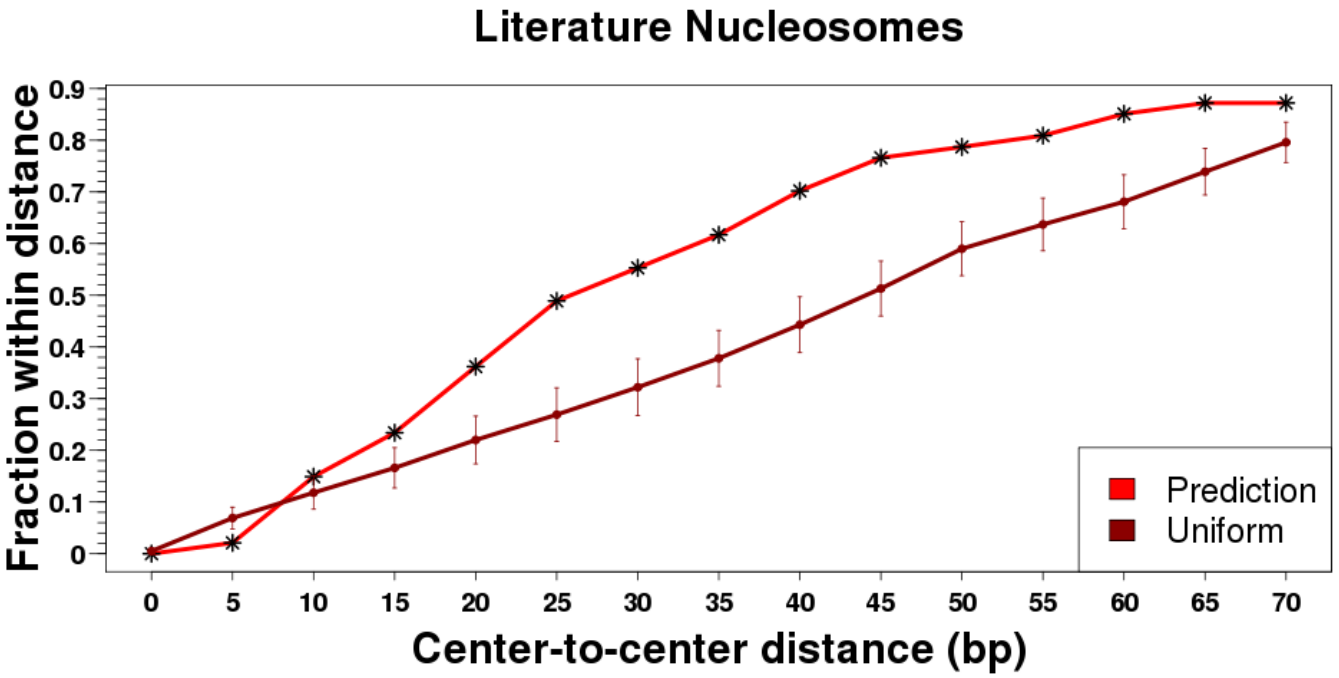

Zawadzki *et al*., Figure S3

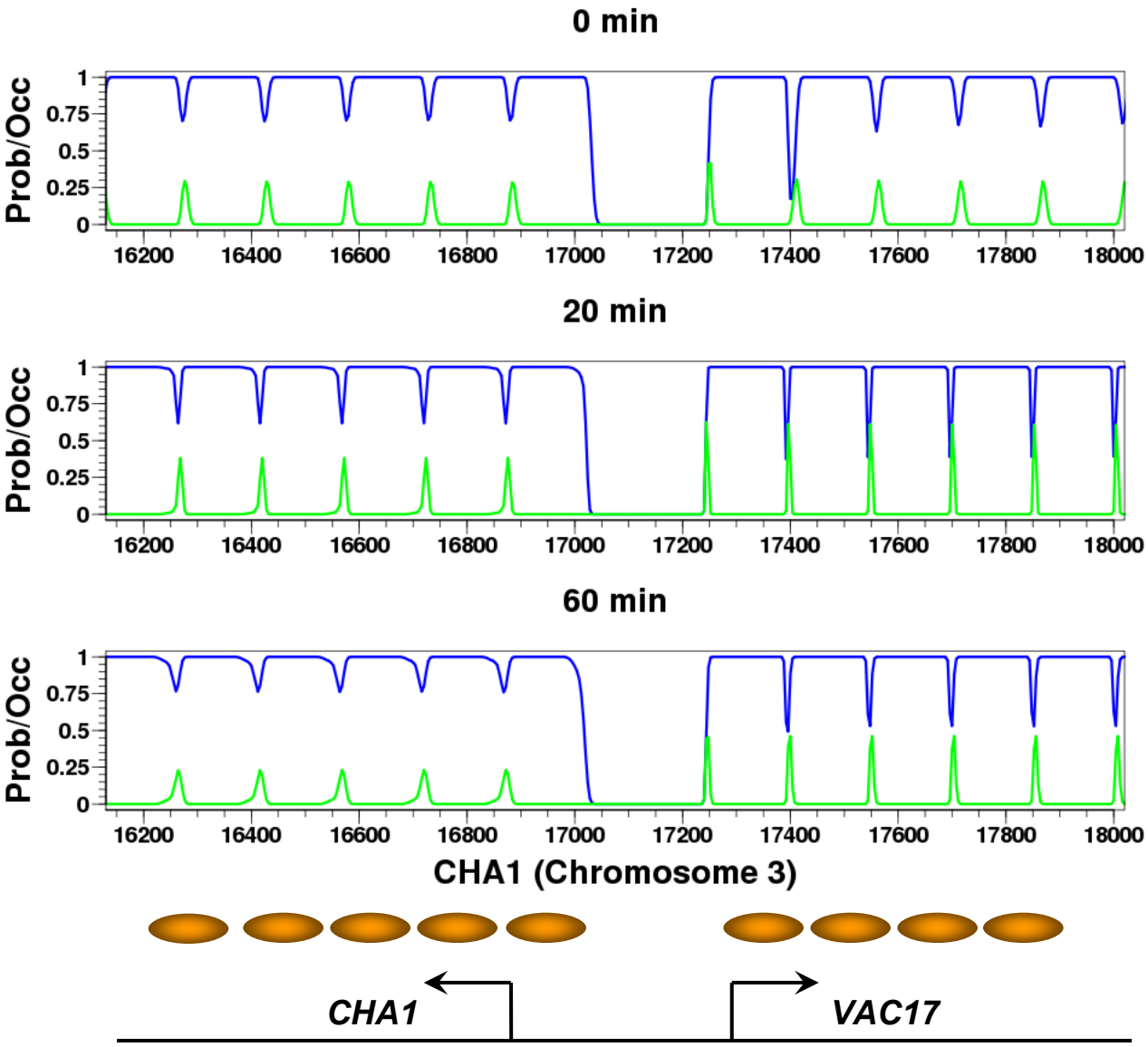

Zawadzki *et al*., Figure S4

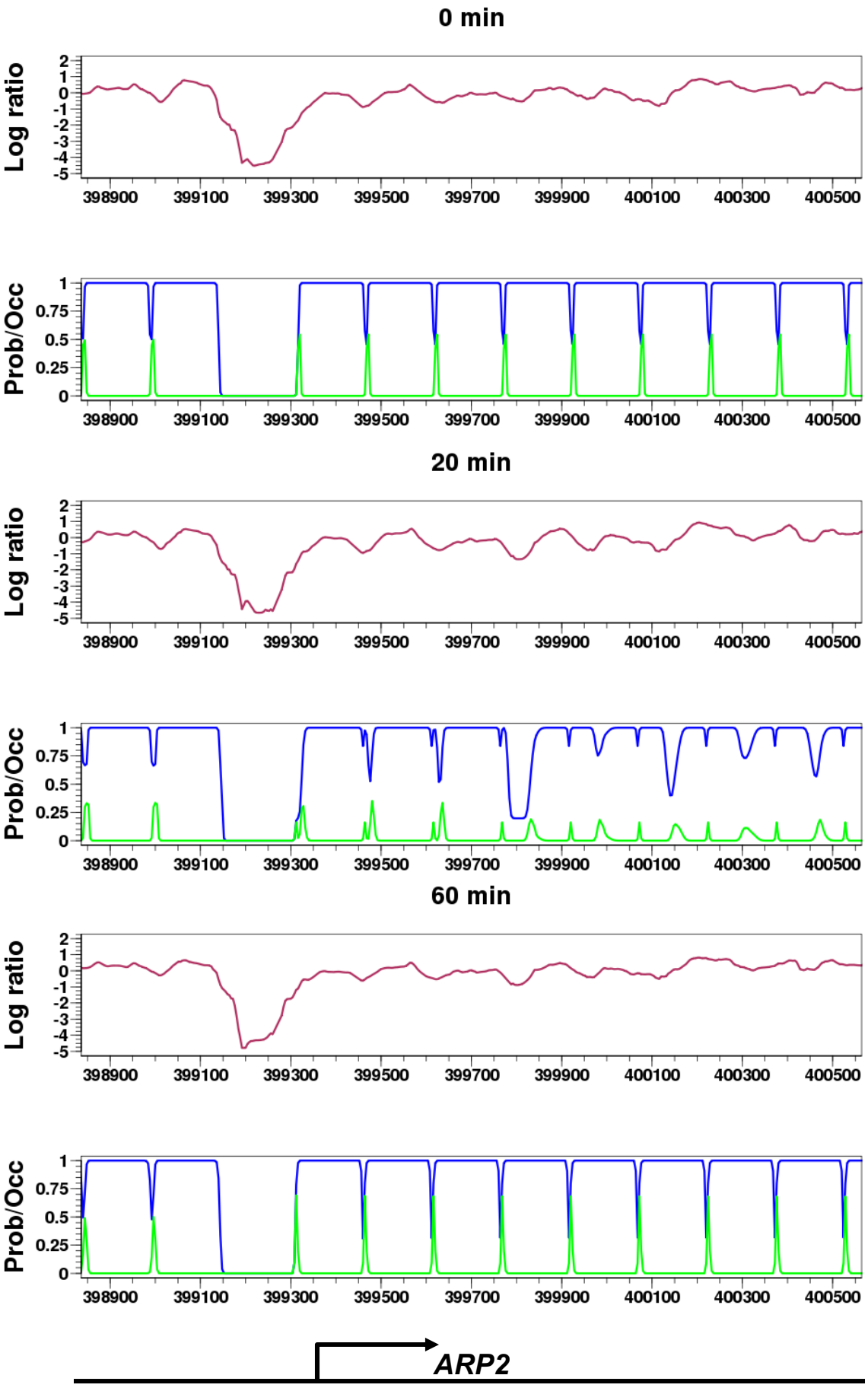

Zawadzki *et al*., Figure S5

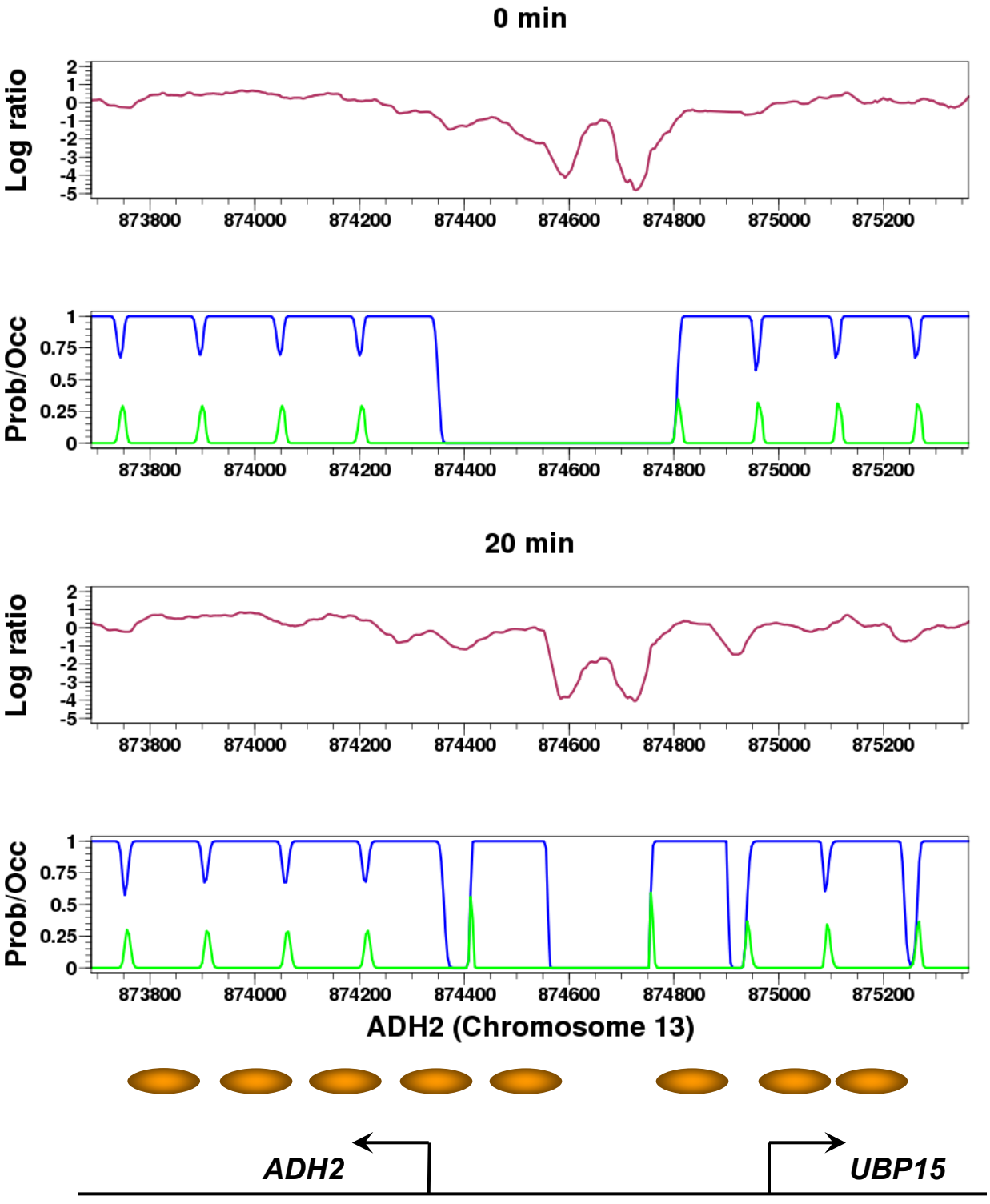

Zawadzki *et al*., Figure S6

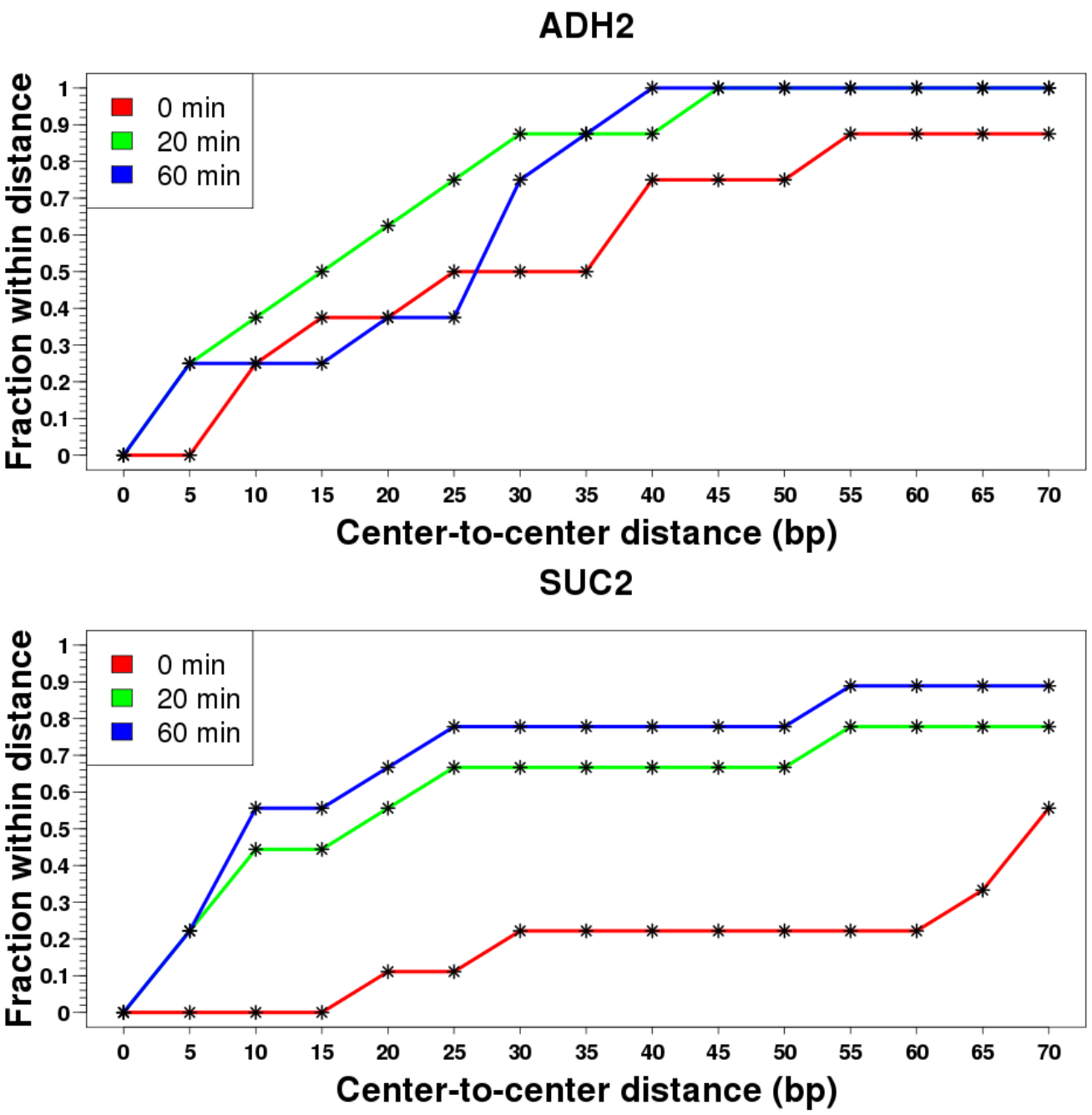

Zawadzki *et al*., Figure S7

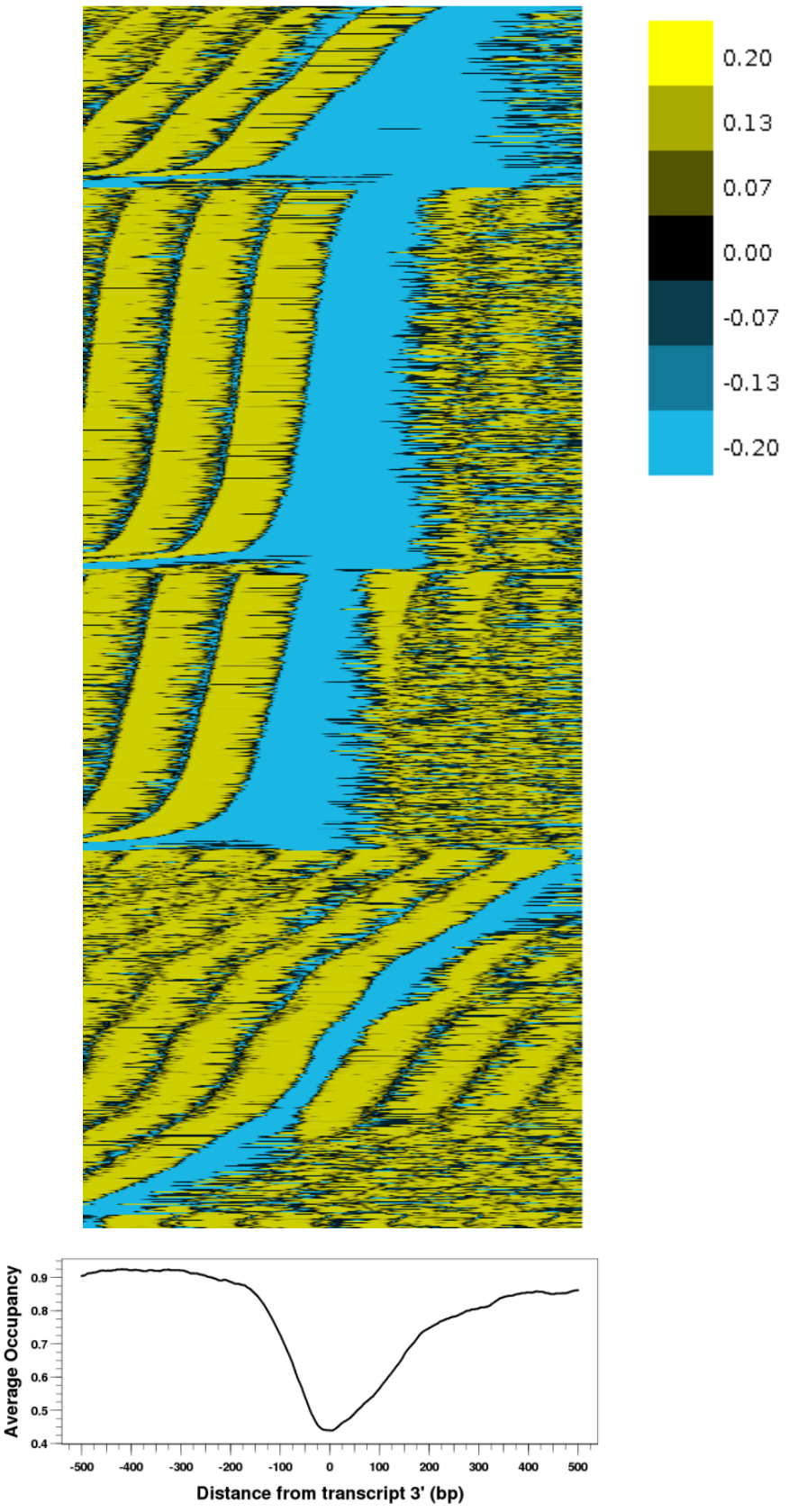

Zawadzki *et al*., Figure S8

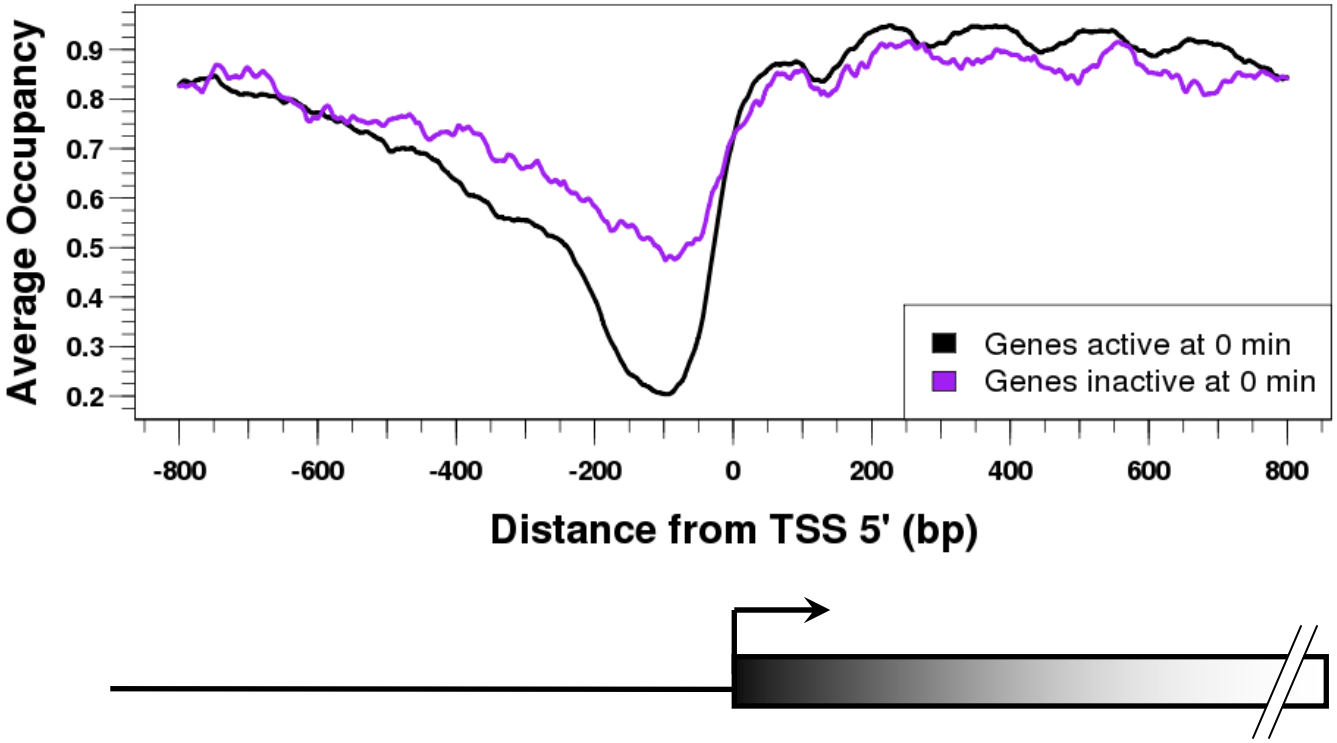

Zawadzki *et al*., Figure S9

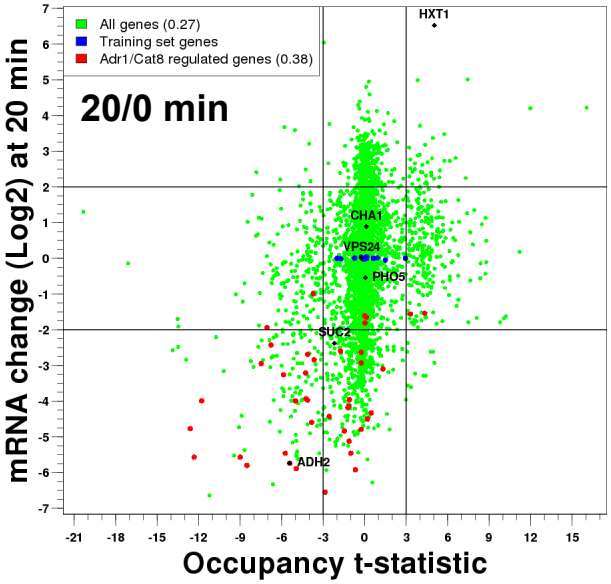

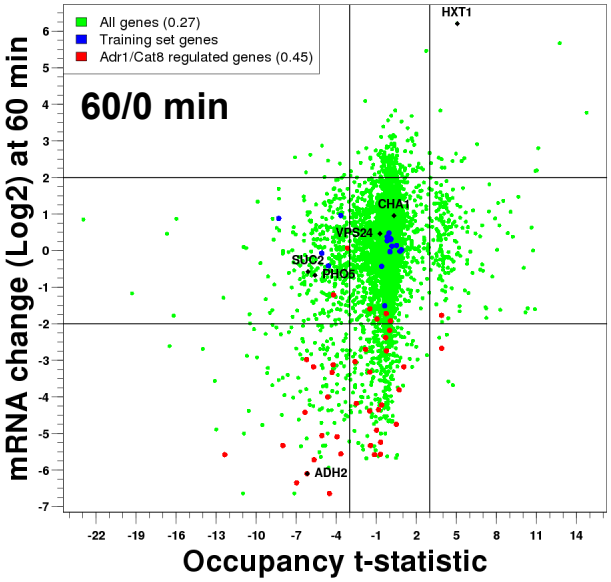

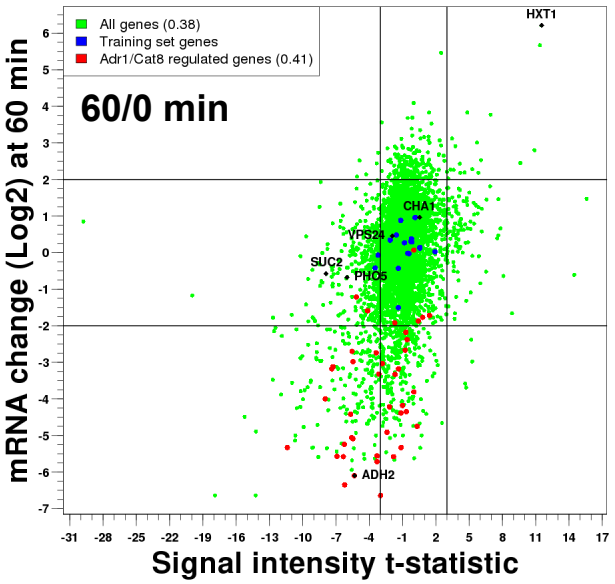

Zawadzki *et al.*, Figure S10

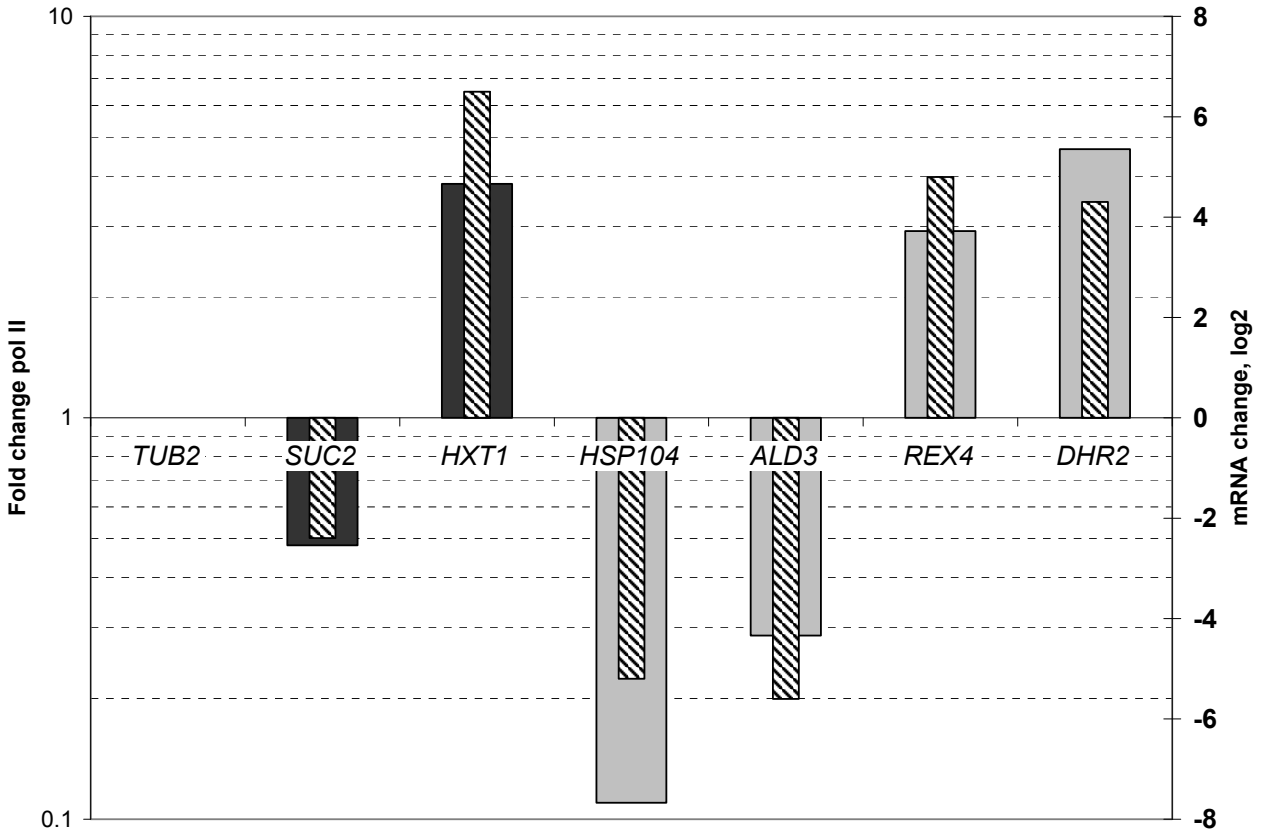

Zawadzki *et al*., Figure S11

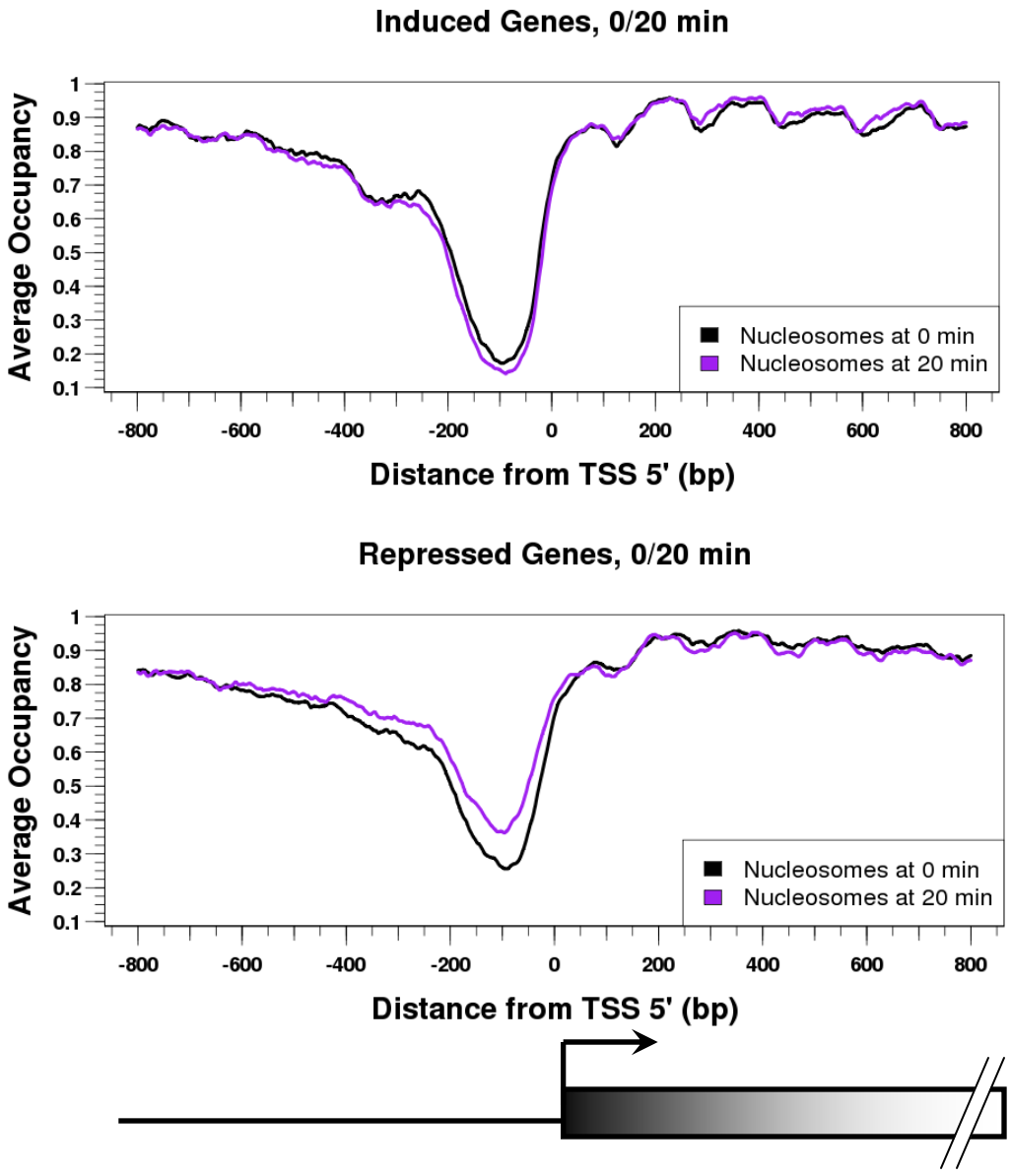

Zawadzki *et al*., Figure S12

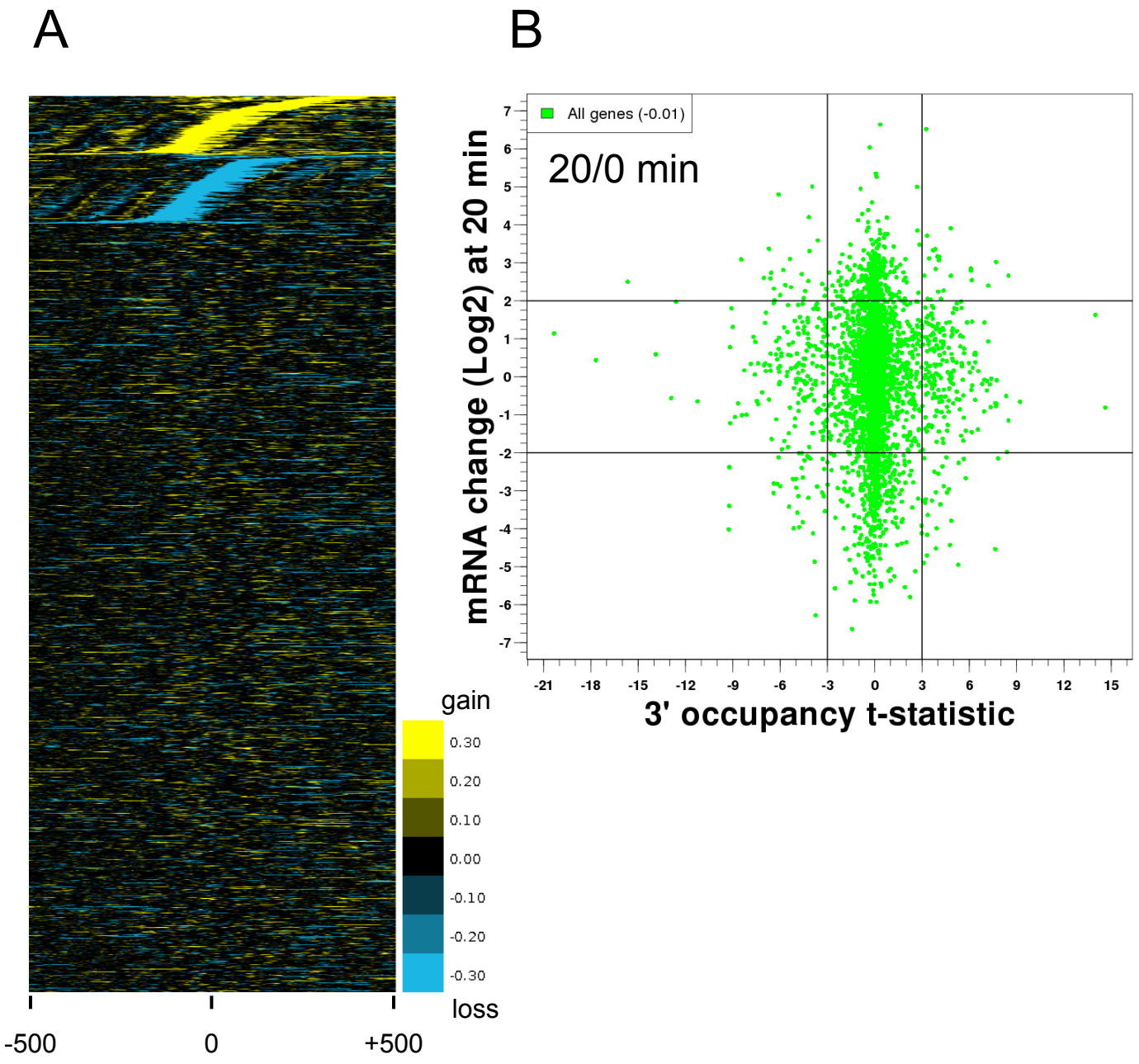

Zawadzki *et al*., Figure S13

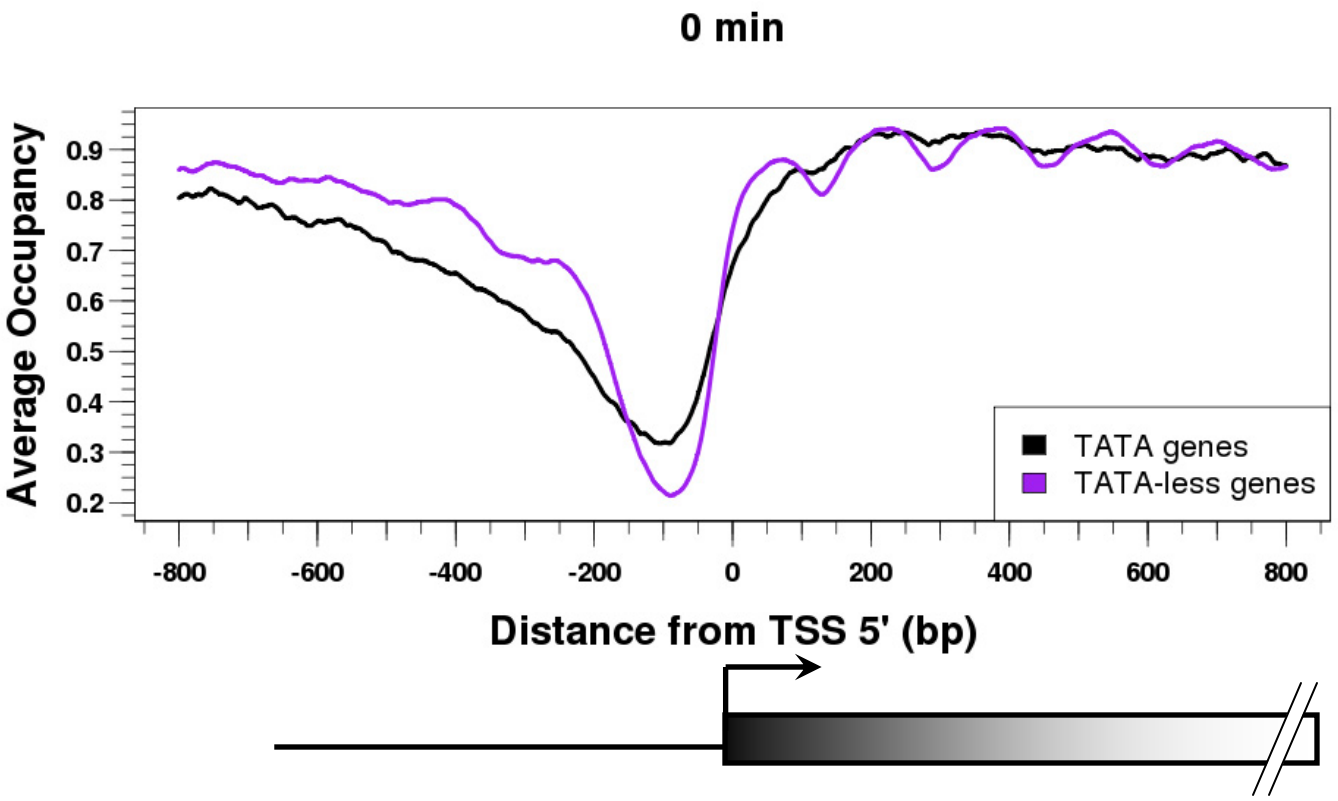

Zawadzki *et al*., Figure S14

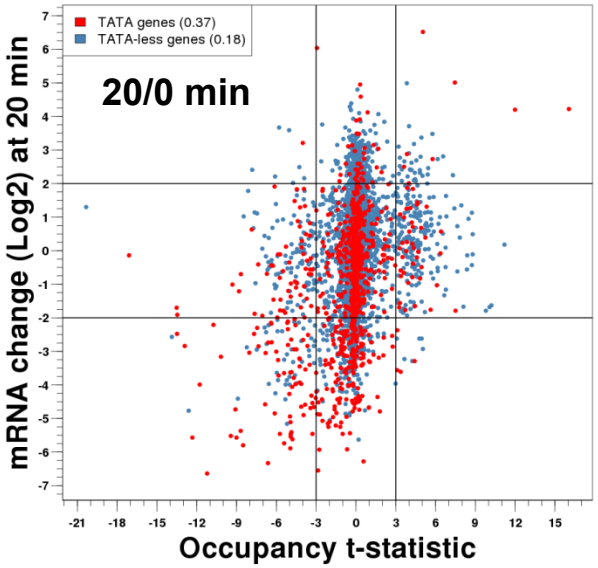

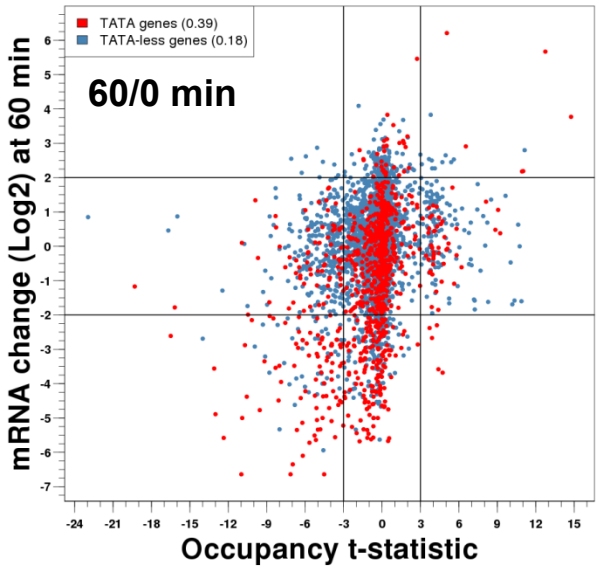

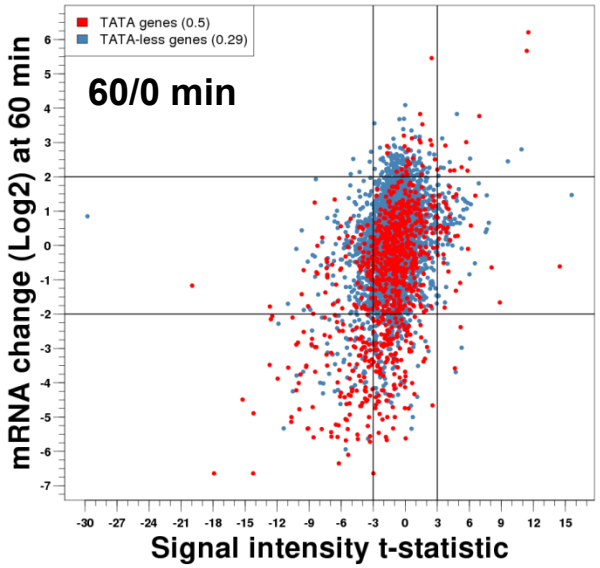

Zawadzki *et al*.,
Figure S15

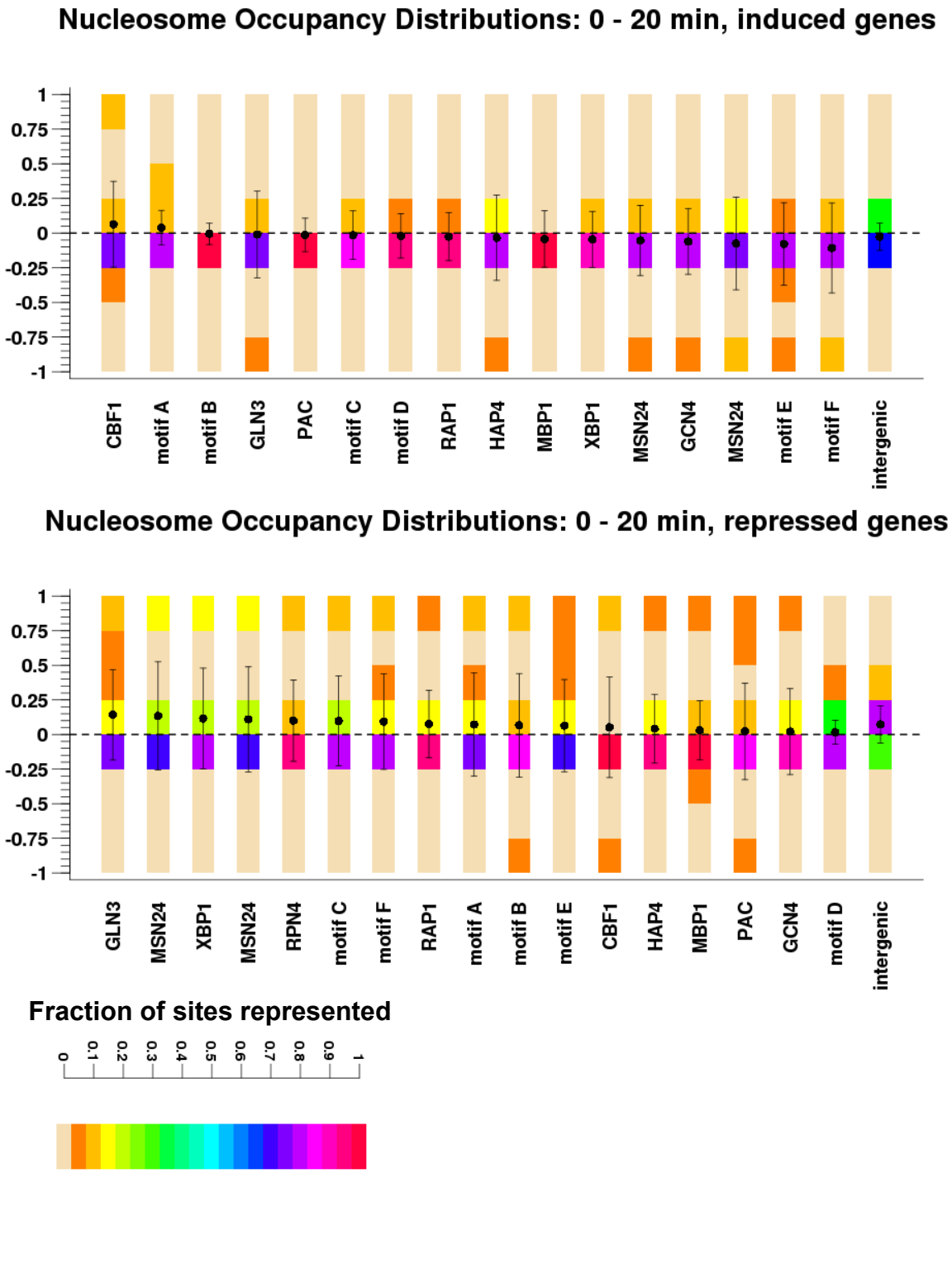

Zawadzki *et al.*,
Figure S16